OPEN

Combined effects of magnetic interaction and domain wall pinning on the coercivity in a bulk $Nd_{60}Fe_{30}Al_{10}$ ferromagnet

X. H. Tan[1], S. F. Chan[1], K. Han[2] & H. Xu[1]

[1]Laboratory for microstructures, School of Materials Science and Engineering, Shanghai University, Shanghai 200444, P. R. China, [2]National High Magnetic Field Laboratory, Florida State University, 1800 E. Paul Dirac Drive, Tallahassee, FL 32310, USA.

Understanding the coercivity mechanism has a substantial impact on developing novel permanent materials. However, the current coercivity mechanisms used widely in permanent alloys cannot explain well the amorphous phase produced hard magnetic behavior of Nd-based bulk amorphous alloys (BAAs). Here, we propose that the coercivity in as-cast $Nd_{60}Fe_{30}Al_{10}$ alloy is from the combination of magnetic interaction and strong pinning of domain walls. Moreover, the role of domain wall pinning is less affected after crystallization, while the magnetic interaction is dependent on the annealing temperature. Our findings give further insight into the coercivity mechanism of Nd-based bulk ferromagnets and provide a new idea to design prospective permanent alloys with coercivity from the combination of magnetic interaction and pinning of domain walls.

P ermanent magnets are fundamental to the technological success in electric machines, and have found applications in a wide range of devices due to their unique ability to deliver magnetic flux into the air gap of a magnetic circuit without continuous expenditure of energy[1]. A breakthrough came in 1984 with a discovery of $Nd_2Fe_{14}B$ phase when Croat *et al* and Sagawa *et al* were able to obtain large coercivity (H_c) in Nd-Fe-B alloys by using melt-spinning and powder metallurgy technique, respectively[2–4]. Since then, Nd-Fe-B magnets with a maximum energy product ($(BH)_{max}$) over 450 kJ/m³ have been exploited and 90% of the limit for the $(BH)_{max}$ can be produced commercially in sintered Nd-Fe-B magnets[5]. However, it appears that the search for novel hard magnetic materials with higher $(BH)_{max}$ has somewhat stagnated and no further breakthrough is in sight. Understanding the coercivity mechanism has a substantial impact on developing novel permanent materials. Three important coercivity mechanisms were used widely in permanent magnets. Nucleation of domain model demonstrates that the nucleation of reverse domains is at surface irregularities and defects with low anisotropy[6,7]. It has been used effectively in sintered $Nd_2Fe_{14}B$, SmCo, bonded $BaFe_{12}O_{19}$ and $Sm_2Fe_{17}N_3$ magnets[8]. The domain wall pinning model shows that the inhomogeneities present in the sample can prevent domain wall motion resulting in high coercivity[9,10]. It has been an important coercivity mechanism in Sm_2Co_{17}-based magnets and melt-spun $Nd_2Fe_{14}B$ alloys[8]. 'Exchange hardening' illustrates that a reasonable high coercivity is obtained resulting from an increase of the nucleation field by the exchange coupling between soft and hard magnetic phase in nanocomposite alloys[11,12]. However, the above three models cannot explain well the amorphous phase produced hard magnetic behavior of Nd-based bulk amorphous alloys (BAAs).

Since the $Nd_{60}Fe_{30}Al_{10}$ bulk amorphous alloy was first reported in 1996[13,14], Nd-Fe-Al based BAAs have been growing interest because of exceptional hard magnetic property at room temperature. It is of interest to note that, although the term *amorphous* is used, the common feature of the microstructure in Nd-based BAAs is the presence of clusters or nanocrystals, which vary in diameter from 1.2 nm to 20 nm, embedded in an amorphous matrix in these materials[15–20]. Despite much effort, the mechanism leading to the hard magnetic behavior of Nd-based bulk amorphous alloys is still under hot debate. In this work, we have studied the relationship between the microstructure and magnetic properties upon annealing of as-cast $Nd_{60}Fe_{30}Al_{10}$ alloy to gain a deeper insight into the coercivity mechanism by a devitrification process. Our results showed that the coercivity in $Nd_{60}Fe_{30}Al_{10}$ alloy resulted from combined effect of magnetic interaction and domain wall pinning. The magnetic interaction
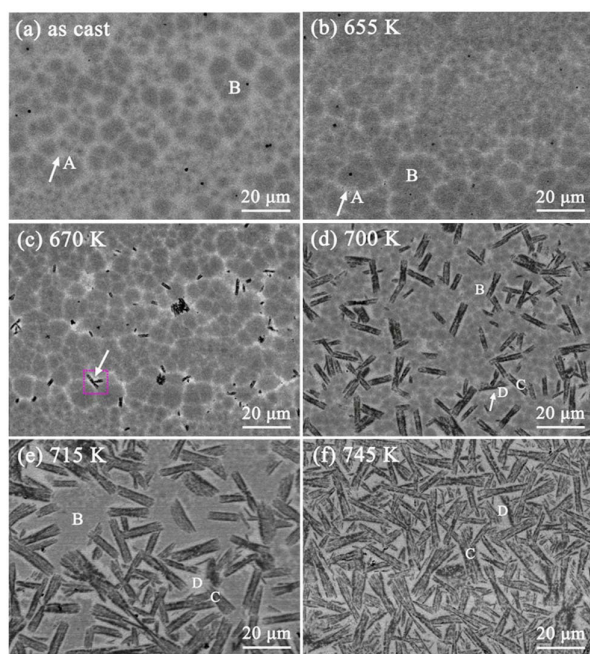
Figure 1 | (a) BSE image of as-cast $Nd_{60}Fe_{30}Al_{10}$ sample; (b)–(f) BSE images of $Nd_{60}Fe_{30}Al_{10}$ samples annealed for 20 min at 655 K, 670 K, 700 K, 715 K and 745 K, respectively.

was sensitive to annealing temperatures, while the role of domain wall pinning was less affected during the crystallization process.

Results

Back-scattered electron (BSE) images of as-cast $Nd_{60}Fe_{30}Al_{10}$ sample and samples annealed at different temperatures for 20 min are shown in Figure 1. Two regions with different contrast (marked as A and B, respectively) was observed, as shown in Fig. 1(a). Further investigation of these two regions by TEM is shown in Figure 2. The insets in Fig. 2(a) and 2(b) are the selected area diffraction patterns (SADPs), which show rings corresponding to hexagonal-close-packed (HCP) Nd phase. The TEM images showed that region A and region B had similar microstructure, that is, both regions had HCP Nd phase of 5–20 nm in size embedded dispersively in an amorphous matrix. However, the energy dispersive spectrometer (EDS) analysis showed that the amorphous phase in region A had the chemistry of $Nd_{60.9}Fe_{30.1}Al_9$, while $Nd_{54}Fe_{35.5}Al_{10.5}$ in region B. When the sample was annealed at 655 K (see Fig. 1(b)), the volume fraction of region A decreased, while that of region B increased. After

annealing at 670 K, the volume fraction of region A further decreased due to decomposing into band-like phase (marked as a square with a dotted line) and Nd-rich phase (marked as an arrow), as shown in Fig. 1(c). When samples were annealed at 700 K and 715 K, the region A disappeared. The growth of band-like phase (marked as C) and Nd-rich phase (marked as D) resulted in the decrease of the volume fraction of region B, as shown in Fig. 1(d) and 1(e), respectively. After the sample was annealed at 745 K, the $Nd_{60}Fe_{30}Al_{10}$ alloy entered a complete crystallization state consisting of the band-like phase and Nd phase. The band-like phase has fine lamellar structure, and its exact composition of individual lamellae could not be accurately measured by EDS. Hence, the EDS gave an average composition of band-like phase as $Nd_{40}Fe_{46}Al_{10}$.

The hysteresis loops of as-cast $Nd_{60}Fe_{30}Al_{10}$ sample and samples annealed for 20 min at various temperatures are shown in Figure 3(a). It is found that as-cast sample showed hard magnetic behavior with an intrinsic coercivity (H_c^i) of 286 kA/m, which was a slight higher than 277 kA/m reported by Inoue[13]. In order to observe the trend of the change of H_c^i, remanence (M_r) and saturation magnetization (M_s) during the annealing process, the percentage change in comparison to the as-cast sample as a function of annealing temperatures is shown in Fig. 3(b). Annealing at 655 K and 670 K decreased H_c^i by less than 20%, while the values of M_r and M_s showed differences less than 3%. When samples were annealed at temperature higher than 700 K, values of M_r and M_s decreased significantly due to the decrease of the volume fraction of region B (see Fig. 1(d)). It is of interest to note that the decrease was much smaller in H_c^i than M_r and M_s. For example, samples annealed at 725 K showed that M_r and M_s had 7% and 27.1%, respectively, while keeping 60.6% H_c^i. It indicates that samples annealed at 725 K still remain as hard magnetic material even though M_r and M_s are low. When the annealing temperature reached 745 K, the sample consisted of Nd phase and band-like phase resulting in a disappearance of hard magnetic properties. Hence, deduced that neither the band-like phase nor the Nd-rich phase were ferromagnetic at room temperature. Our measured Curie temperature (T_C) for as-cast sample and samples annealed at various temperatures had a same value, 526 K, demonstrating that these samples had the same magnetic phase. Moreover, it is close to the T_C of amorphous phase[13] indicating that the amorphous phase is only the magnetic phase. To further understand the coercivity mechanism, the magnetic interaction was investigated.

In as-cast sample and samples annealed at 655 K, 670 K and 700 K, we found that the ratio of M_r and M_s was more than 0.5 suggesting the presence of magnetic interaction[11]. An effective method of understanding the phenomenon of magnetic interaction is via so called the Henkel plot[21]. Wohlfarth showed that for non-interacting single-domain particles[22],
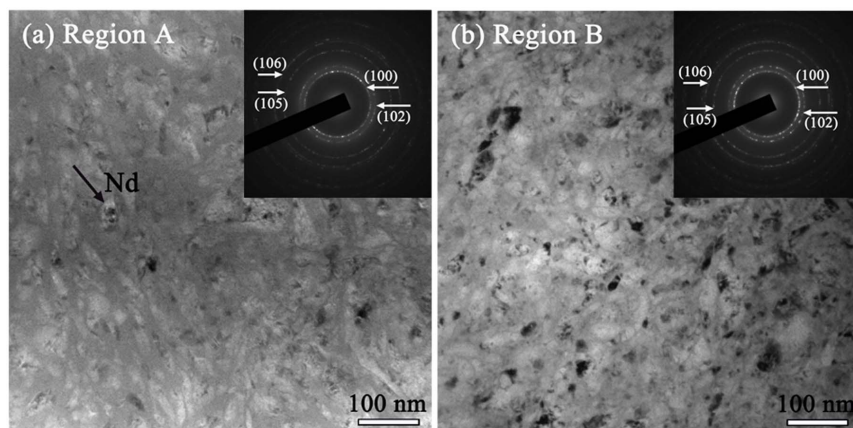

Figure 2 | TEM images of region A (a) and region B (b) of as-cast $Nd_{60}Fe_{30}Al_{10}$ sample.

$$M_d(H) = 1 - 2M_r(H) \qquad (1)$$

where $M_d(H)$ and $M_r(H)$ are the reduced magnetization and reduced remanent magnetization, respectively.

Eq. (1) should show a straight line for non-interacting domain particles. It was first noted by Henkel the experimental variation gave characteristic plots which showed both positive and negative curvature[21]. The positive deviation with the curve concave downwards indicates the presence of magnetic interaction. Figure 4 shows Henkel plots of as-cast $Nd_{60}Fe_{30}Al_{10}$ alloy and the samples annealed in the temperature range 655 K–725 K for 20 min. It is seen that, for the as-cast sample, a Henkel plot crosses the non-interaction line (marked as a dash line in Fig. 4). A positive deviation (marked as an arrow) from the linear plot suggests the presence of strong magnetic interactions. However, for samples annealed at 655 K, 670 K and 700 K, a reduction of magnetic interaction was observed. When the samples were annealed at temperatures higher than 700 K, the magnetic interaction was very weak, which is not considered as the origin of coercivity in this case. However, it is worthy of note that these samples still remain as a hard material. For example, the value of H_c^i is 214.7 kA/m, 202.3 kA/m and 173.4 kA/m for samples annealed at 700 K, 715 K and 725 K, respectively. It indicates that the magnetic interaction cannot explain well the origin of coercivity of the $Nd_{60}Fe_{30}Al_{10}$ alloy.
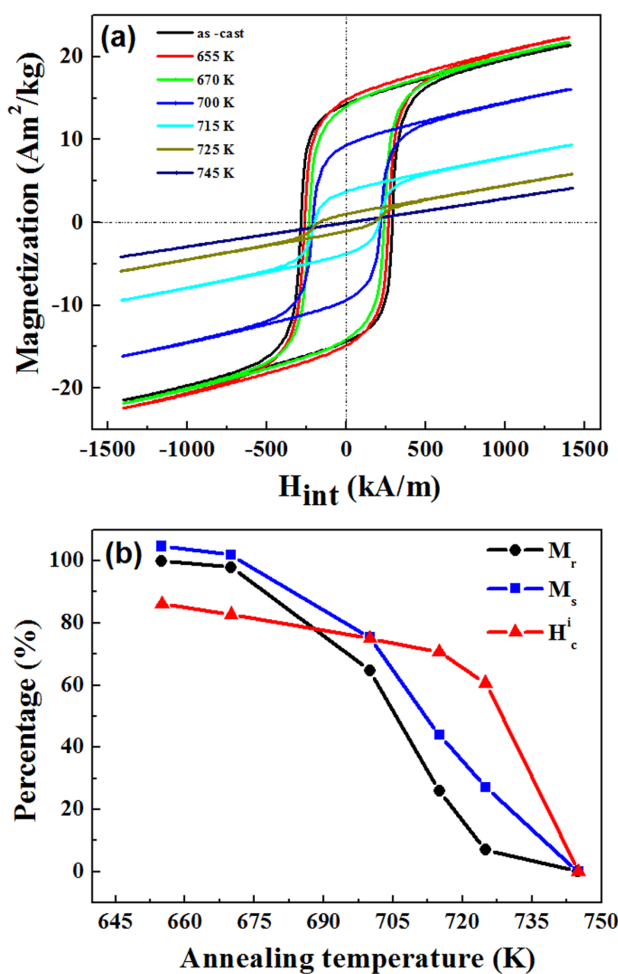
For the case of strong pinning of domain walls developed by Gaunt[23], the intrinsic coercivity, H_c^i, as a function of temperature, T, is given by

$$\left(\frac{H_c^i}{H_0}\right)^{1/2} = 1 - \left(\frac{75k_BT}{4bf}\right)^{2/3} \qquad (2)$$

where H_0 is the critical field (the field required to release a domain wall from a pinning centre) at $T = 0$, k_B is Boltzmann constant, f the maximum restoring force per pin, and $4b$ is the interaction range of a pin. The domain wall width, δ_w, can be equated with $4b$. The temperature dependence of the coercivity in the Nd-based alloys found that the coercivity reached a maximum at temperature T_{peak} in the temperature range 10 K–425 K[24–27]. Investigations showed that the covercivity above T_{peak} followed Gaunt's strong pinning of domain walls[26,27]. Hence, in our work, only values of coercivity above T_{peak} are considered. The temperature dependence of the coercivity in the temperature range 140–300 K is shown in Figure 5. The simple linear relationship between $(H_c^i)^{1/2}$ and $T^{2/3}$ demonstrates a very good agreement with the strong domain pinning model in as-cast $Nd_{60}Fe_{30}Al_{10}$ sample and samples annealed in the temperature range 655 K–725 K. In this case, coercivity arises from impediments to domain wall motion due to magnetic inhomogeneities or pinning centers, including precipitates or any region with magnetic property different from the matrix. Hence, combined with Henkel plot result, we propose that the origin of coercivity in as-cast $Nd_{60}Fe_{30}Al_{10}$ bulk amorphous alloy is from a combination of magnetic interaction and strong pinning of domain walls.

Discussion

The origin of magnetic interaction is continued debate in Nd-based alloys. McCallum and his co-workers suggested it was from the coupling of δ-phase ($Nd_6Fe_{13-x}Al_{1+x}$, $2 < x < 5.5$) to the ferromagnetic matrix in an "exchange-bias" type manner in Nd-Fe-Al alloys[18], while Wei et al confirmed that the interaction was from exchange coupling between magnetic clusters by observation of domain walls using magnetic-force microscopy in the $Nd_{60}Fe_{20}Al_{10}Co_{10}$ alloy[28]. In our work, the magnetic interaction has a close relationship with the presence of region A and region B in Fig. 1(a). Although the TEM result showed that region A and region B had similar microstructure with HCP Nd phase in size of 5–20 nm embedded in the amorphous phase, the EDS analysis have showed that the chemistry of the amorphous phase in region A and region B was different. Since the
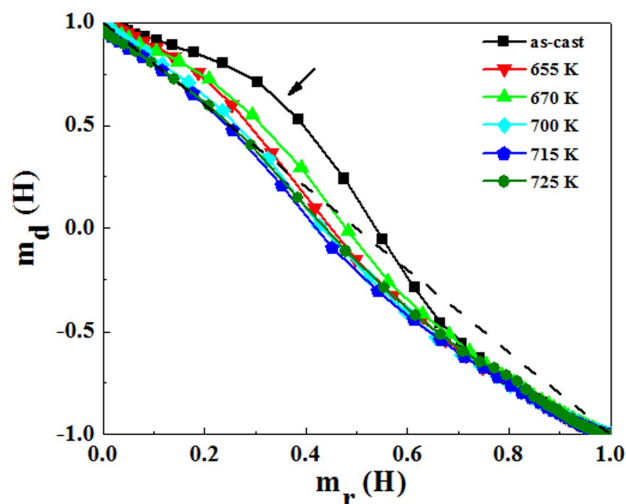

Figure 3 | (a) Hysteresis loops of as-cast $Nd_{60}Fe_{30}Al_{10}$ alloy and the samples annealed for 20 min at 655 K, 670 K, 700 K, 715 K, 725 K and 745 K, respectively. (b) The percentage change of M_r, M_s and H_c^i in comparison to the as-cast sample as a function of annealing temperature.

Figure 4 | Henkel plots of as-cast $Nd_{60}Fe_{30}Al_{10}$ alloy and samples annealed for 20 min at 655 K, 670 K, 700 K, 715 K and 725 K, respectively.
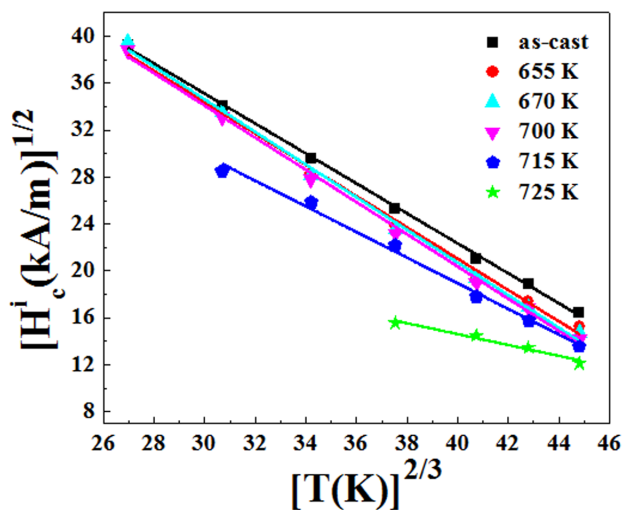
Figure 5 | $(H_c^i)^{1/2}$ **as a function of** $T^{2/3}$ **in the temperature range 140–300 K for as-cast** $Nd_{60}Fe_{30}Al_{10}$ **alloy and annealed for 20 min at 655 K, 670 K, 700 K, 715 K and 725 K, respectively.**

amorphous phase is the only magnetic phase in the alloy, it is deduced that the magnetic interaction is sensitive to the presence of the amorphous phase with different composition. In the role of domain wall pinning of the as-cast $Nd_{60}Fe_{30}Al_{10}$ alloy, it does appear that an effect of pinning domain wall relates to the size of the crystallites. When the size of particles or crystallites is comparable with the domain wall, it is expected that it will pin domain walls, as when this condition applies pinning is known to be most pronounced[8]. Hence, in our case, nanosize Nd phase can act as pinning centers, due to the size is comparable to the domain wall width ($\delta_w \approx 11$ nm[26]).

It is interesting to note that the role of domain wall pinning is less affected during crystallization, while the magnetic interaction is dependent on annealing temperature. When samples were annealed at 655 K and 670 K, the decrease of the magnetic interaction was observed. When samples were annealed above 700 K, the magnetic interaction was depressed due to significant decrease of the volume fraction of region A. In this case, the negative deviation with the curve concave upwards was observed in Henkel plot (see Fig. 4), which may result from the impedance of domain walls[29]. Given the strong evidence for the pinning model shown in Fig. 5, we conclude the role of strong pinning of domain walls is dominant in samples annealed above 700 K.

In summary, our results showed that magnetic property had a close relationship with the microstructure during the devitrification process in the $Nd_{60}Fe_{30}Al_{10}$ alloy. The values of M_r and M_s had minor change in samples annealed at 655 K and 670 K, whist showed significant decrease after annealing higher than 700 K. However, the samples annealed over 700 K still remained as hard magnetic material even though M_r and M_s were low. An unusual coercivity mechanism is proposed, that is, the coercivity in the $Nd_{60}Fe_{30}Al_{10}$ alloy is from the combination of magnetic interaction and strong pinning of domain walls. The latter one is less affected during crystallization, while the magnetic interaction is dependent on annealing temperature. When annealing temperatures were higher than 700 K, the magnetic interaction was depressed and the role of domain walls pinning was dominant. The present work provides a new idea to develop prospective permanents alloys with good magnetic properties.

Methods

Alloy ingots with a nominal composition of $Nd_{60}Fe_{30}Al_{10}$ were prepared by arc-melting 99.99% pure Nd, Fe and Al in a high pure argon atmosphere. The cylindrical rods of 2 mm in diameter and 50 mm in length were prepared by copper mold suction casting. The as-cast samples were annealed at various temperatures in the range 655–745 K for 20 min in a vacuum furnace with a pressure of less than 2×10^{-3} Pa. The microstructure of samples was studied by a scanning electron microscope (SEM, SU1510) equipped with an in-situ energy dispersive spectrometer (EDS) and transmission electron microscope (TEM, JEM 2010F) with a field emission electron gun operating at 200 kV. TEM samples were made by a focus ion beam (FIB) (FEI Helios 600i). Magnetic hysteresis loops at room temperature were performed using a Lake Shore 7407 vibrating sample magnetometer (VSM) with a maximum magnetic field of 1.8 T. The Henkel plot was determined from the measurement of isothermal remanence magnetization (IRM) and DC demagnetization (DCD) curve. The samples for IRM and DCD curves were virgin state. The detailed measurement of IRM and DCD curve was introduced in reference 30. The temperature dependence of the coercivity was measured by using a Quantum Design Physical Property Measurement System (PPMS) equipped with a 9 T magnet. Major hysteresis loops were measured in the range 140 K to 260 K, and the intrinsic coercivity determined from each hysteresis loop.

1. Sugimoto, S. Current status and recent topics of rare-earth permanent magnets. *J. Phys. D: Appl. Phys.* **44**, 064001 (2011).
2. Croat, J. J., Herbst, J. F., Lee, R. W. & Pinkerton, F. E. Pr-Fe and Nd-Fe-based materials: A new class of high-performance permanent magnets (invited). *J. Appl. Phys.* **55**, 2078–2082 (1984).
3. Croat, J. J., Herbst, J. F., Lee, R. W. & Pinkerton, F. E. High-energy product Nd-Fe-B permanent magnets. *Appl. Phys. Lett.* **44**, 148–149 (1984).
4. Sagawa, M., Fujimura, S., Togawa, N., Yamamoto, H. & Matsuura, Y. New material for permanent magnets on a base of Nd and Fe (invited). *J. Appl. Phys.* **55**, 2083–2087 (1984).
5. Gutfleisch, O. *et al.* Magnetic Materials and Devices for the 21st Century: Stronger, Lighter, and More Energy Efficient. *Adv. Mater.* **23**, 821–842 (2011).
6. Durst, K. D. & Kronmüller, H. The coercive field of sintered and melt-spun NdFeB magnets. *J. Magn. Magn. Mater.* **68**, 63–75 (1987).
7. Herbst, J. F. $R_2Fe_{14}B$ materials: Intrinsic properties and technological aspects. *Rev. Mod. Phys.* **63**, 819–898 (1991).
8. Skomski, R. & Coey, J. M. D. Permanent Magnetism, Institute of Physics Publishing, Bristol and Philadelphia, 1999.
9. Hadjipanayis, G. C., Lawless, K. R. & Dickerson, R. C. Magnetic hardening in iron-neodymium-boron permanent magnets. *J. Appl. Phys.* **57**, 4097–4099 (1985).
10. Pinkerton, F. E. & Wingerden, D. J. V. Magnetization process in rapidly solidified neodymium-iron-boron permanent magnet materials. *J. Appl. Phys.* **60**, 3685–3690 (1986).
11. Coehoorn, R., de Mooji, D. B. & de Waard, C. Meltspun permanent magnet materials containing Fe_3B as the main phase. *J. Magn. Magn. Mater.* **80**, 101–104 (1989).
12. Hadjipanayis, G. C. Nanophase hard magnets. *J. Magn. Magn. Mater.* **200**, 373–391 (1999).
13. Inoue, A., Zhang, T., Zhang, W. & Takeuchi, A. Bulk Nd-Fe-Al Amorphous Alloys with Hard Magnetic Properties. *Mater. Trans. JIM* **37**, 99–108 (1996).
14. Inoue, A., Zhang, T., Takeuchi, A. & Zhang, W. Hard Magnetic Bulk Amorphous Nd-Fe-Al Alloys of 12 mm in Diameter Made by Suction Casting. *Mater Trans., JIM* **37**, 636–640 (1996).
15. Schneider, S., Bracchi, A., Samwer, K., Seibt, M. & Thiyagarajan, P. Microstructure-controlled magnetic properties of the bulk glass-forming alloy $Nd_{60}Fe_{30}Al_{10}$. *Appl. Phys. Lett.* **80**, 1749–1751 (2002).
16. Sun, Z. G., Kumar, G., Löser, W., Eckert, J. & Schultz, L. Effect of Y addition on the microstructure and magnetic properties of $Nd_{60-x}Y_xFe_{30}Al_{10}$ mould-cast alloys. *J. Alloys Compd.* **366**, 248–253 (2004).
17. Bracchi, A., Samwer, K., Schneider, S. & Löffler, J. F. Random anisotropy and domain-wall pinning process in the magnetic properties of rapidly quenched $Nd_{60}Fe_{30}Al_{10}$. *Appl. Phys. Lett.* **82**, 721–723 (2003).
18. McCallum, R. W., Lewis, L. H., Kramer, M. J. & Dennis, K. W. Magnetic aspects of the ferromagnetic "bulk metallic glass" alloy system Nd-Fe-Al. *J. Magn. Magn. Mater.* **299**, 265–280 (2006).
19. Tan, X. H. *et al.* Microstructure and magnetic viscosity of bulk amorphous $Nd_{60}Fe_{20}Al_5Co_{10}B_5$ alloy. *J. Appl. Phys.* **109**, 083927 (2011).
20. Tan, X. H., Collocott, S. J., Liu, H. W., Xiong, X. Y. & Xu, H. Structural analysis of nanocrystals and their role in the coercivity mechanism of Nd-Fe-Al-Dy bulk amorphous ferromagnets. *J. Magn. Magn. Mater.* **343**, 27–31 (2013).
21. Henkel, O. Remanenzverhalten und Wechselwirkungen in hartmagnetischen Teilchenkollektiven. *Phys. Stat. Sol. (b)* **7**, 919–929 (1964).
22. Wohlfarth, E. P. Relations between Different Modes of Acquisition of the Remanent Magnetization of Ferromagnetic Particles. *J. Appl. Phys.* **29**, 595–596 (1958).
23. Gaunt, P. Ferromagnetic domain wall pinning by a random array of inhomogeneities. *Philos. Mag. B* **48**, 261–276 (1983).
24. Turtelli, R. S. *et al.* Coercivity mechanism in $Nd_{60}Fe_{30}Al_{10}$ and $Nd_{60}Fe_{20}Co_{10}Al_{10}$ alloys. *Phy. Rev. B* **66**, 054441 (2002).
25. Kumar, G. *et al.* Magnetic properties of amorphous Nd-Fe-Co-Al alloys. *Mater. Sci. Eng. A* **375–377**, 1083–1086 (2004).
26. Tan, X. H., Collocott, S. J. & Xu, H. Sweep rate and temperature dependence of the coercivity in $Nd_{60-x}Fe_{30}Al_{10}Dy_x$, x = 0, 2 and 4, bulk amorphous ferromagnets. *J. Magn. Magn. Mater.* **324**, 2565–2571 (2012).

27. Kumar, G., Eckert, J., Roth, S., Müller, K.-H. & Schultz, L. Coercivity mechanism in mold-cast $Nd_{60}Fe_xCo_{30-x}Al_{10}$ bulk amorphous alloys. *J. Alloys Compd.* **348**, 309–313 (2003).

28. Wei, B. C. *et al.* Domain structure of a $Nd_{60}Al_{10}Fe_{20}Co_{10}$ bulk metallic glass. *Phys. Rev. B* **64**, 012406 (2001).

29. McMichael, R. D., Vajda, F. & Torre, E. D. Demagnetized-state dependence of Henkel plots. II. Domain wall motion. *J. Appl. Phys.* **75**, 5692–5694 (1994).

30. García-Otero, J., Porto, M. & Rivas, J. Henkel plots of single-domain ferromagnetic particles. *J. Appl. Phys.* **87**, 7376–7381 (2000).

Acknowledgments

Author contributions

S.F. Chan carried out the experiments. X.H. Tan, H. Xu and K. Han analyzed the data and had discussions about results. X.H. Tan and H. Xu wrote the manuscript.

Additional information